Supplemental Methods

Primer sequences

Sry	forward 5' CAGAATCCCAGCATGCAAAATAC 3'
	reverse 5' CGGCTTCTGTAAGGCTTTTCC 3'
	probe 5' AGATCAGCAAGCAGCTGGGATGCA 3'
18s RNA	forward 5' TTTCGGAACTGAGGCCATGA 3'
	reverse 5' GCAAATGCTTTCGCTCTGGTC 3'
STAT3	forward 5' GTCACATGCCACGTTGGTGTTTCA 3'
	reverse 5' CGGGCAATTTCCATTGGCTTCTCA 3'
$p21^{Cip1}$	forward 5' GACCTGGGAGGGGACAAGAG 3'
	reverse 5' TTCTCTTGCAGAAGACCAATC 3'
p65	forward 5' CTGATGTGCATCGGCAAG 3'
	reverse 5' TGCTGGGAAGGTGTAGGG 3'
SDF-1	forward 5' ACACTCCAAACTGTGCCCTTCAGA 3'
	reverse 5' ATGCTGGCAAACCTTAGCATGACC 3'
Fractalkine	forward 5' CCAGGGTCCTTTCCTGTCTCT 3'
	reverse 5' TGGAGAATGCTATGGGAGTTCTG 3'
CD3	forward 5' TGCCTCAGAAGCATGATAAGC 3'
	reverse 5' GCCCAGAGTGATACAGATGTCAA 3'
CD115	forward 5' ATCTGTTCCCGTCCTCACAG 3'
	reverse 5' ACTGCCATTGCTCACACATC 3'

gp130 forward 5’ CTCACCTGCAACATCCTGTCCT 3’

reverse 5’ GCTGACCATACATGAAGTGCCA 3’

For RANTES qRT-PCR we generally used the following primers:

forward 5’ TCGTGCCCACGTCAAGGAGTATTT 3’

reverse 5’ TCTTCTCTGGGTTGGCACACACTT 3’

Alternatively, for qRT-PCR involving VSMCs/tissues from *RANTES*$^{-/-}$ mice, the following deletion-specific RANTES primers were used:

forward 5’ TCTGCCGCGGGTACCATGAAGAT 3’

reverse 5’ GAGCACTTGCTGCTGGTGTAGAAA 3’

ChIP NF-κB binding site #1 of *RANTES* promoter:

forward 5’ TGACACAAGTGTGGTCTGTTTCTG 3’

reverse 5’ AGGTAGCAGGGAGCTGTTGTCTTA 3’

ChIP NF-κB binding site #2 of *RANTES* promoter:

forward 5’ ACAGCAACAAGTGTTTGGTGTCTT 3’

reverse 5’ TTTATAGGGAGCCAGGGTAGCAGA 3’

β-actin genomic control (ChIP):

forward 5’ TTTCCCTGAGCAGCTTGTCA 3’

reverse 5’ CTGGGCCGTTAGCTAGTGTC 3’

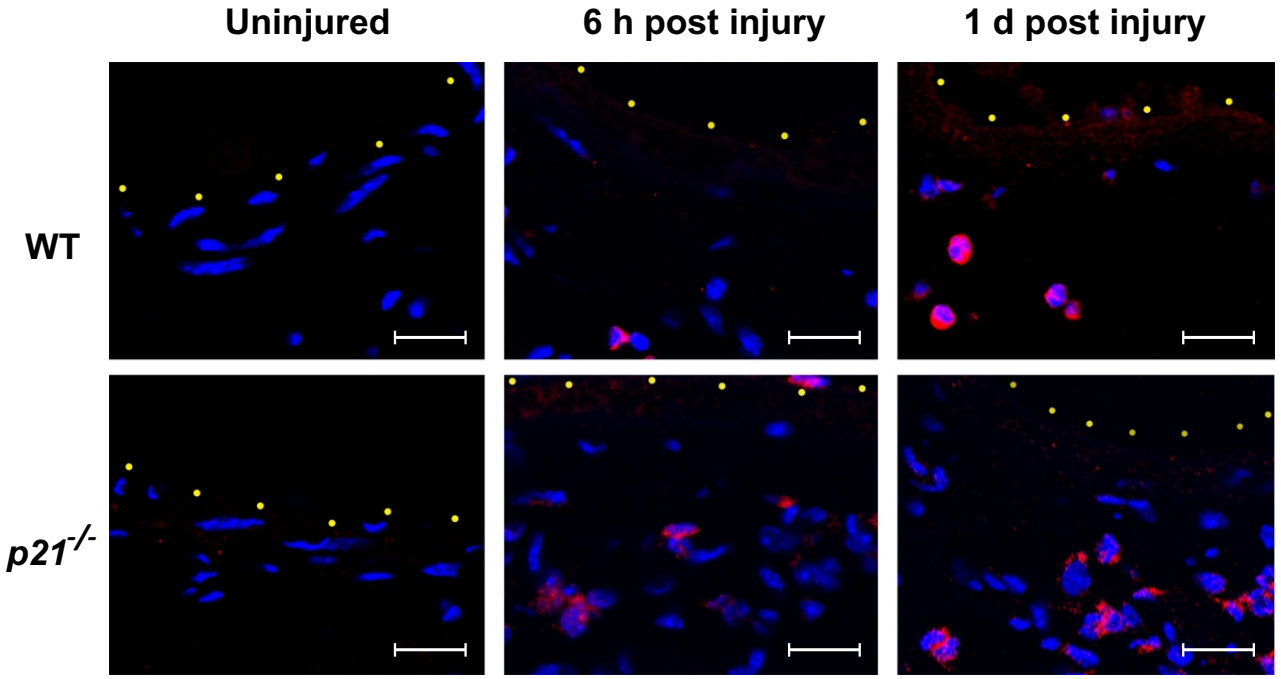

Supplemental Figure 1

Representative alternative higher-power confocal microscopic images showing $CD3^+$ cells (red) in femoral artery sections from WT and *p21*$^{-/-}$ mice in uninjured vessels and at 6 h and 1 d following arterial wire injury. Nuclei (blue) were stained with DAPI. The vessel lumen (upper aspect of each panel) is marked by yellow dots. Scale bars = 20 m.

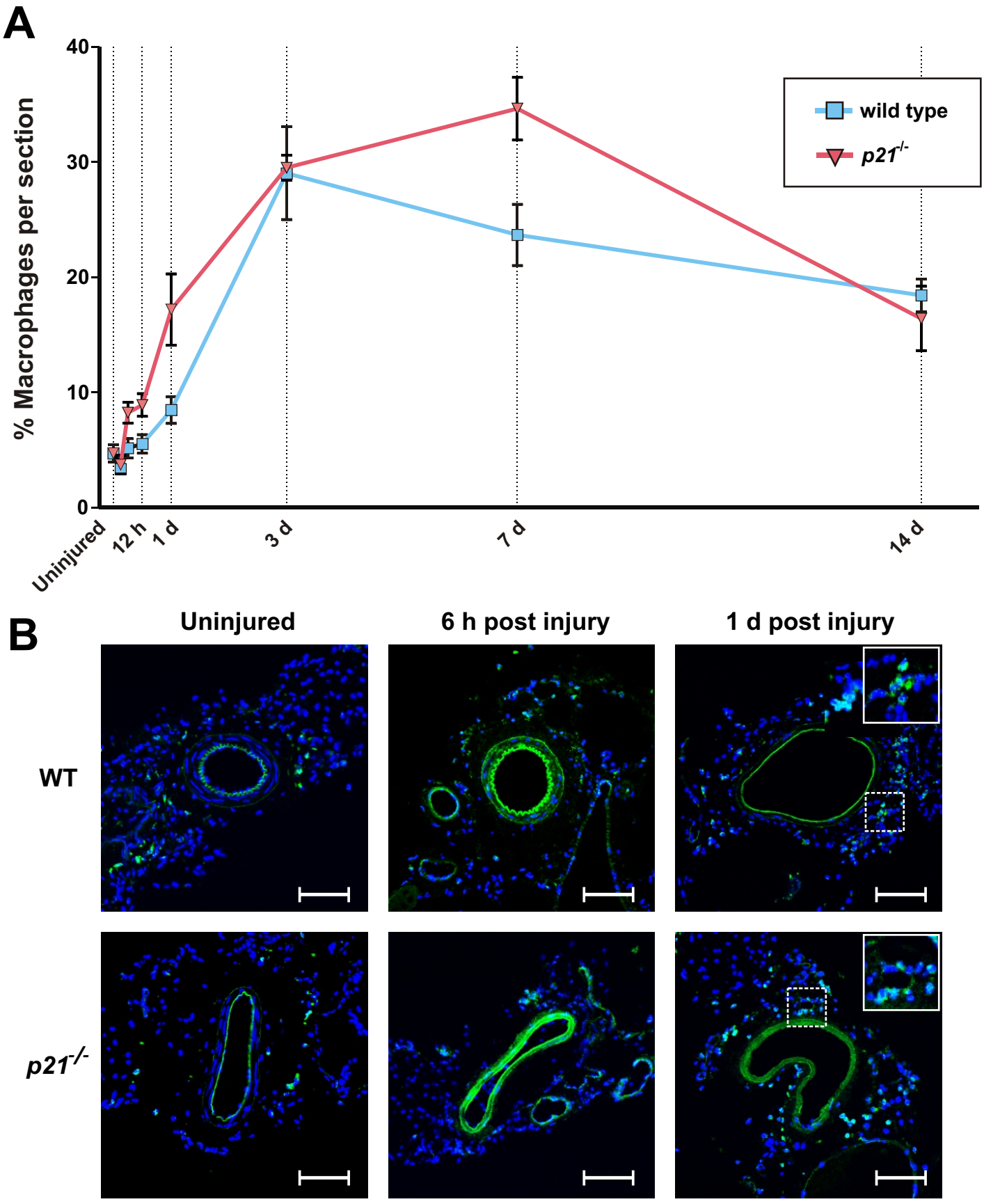

Supplemental Figure 2

CD115^{+} macrophage infiltration following arterial wire injury. **(A)** Relative CD115^{+} macrophage infiltration in WT and *p21*$^{-/-}$ mice. **(B)** Representative corresponding confocal microscopic images of femoral artery sections showing CD115^{+} macrophages (green) in uninjured vessels and at 6 h and 1 d following arterial wire injury, with the dashed square indicating an area of higher magnification shown in the upper-right corner for the 1 d images (width of inset square = 70 m). Nuclei (blue) were stained with DAPI. Arterial elastic laminae are visible in green due to auto-fluorescence. Scale bars = 100 m.

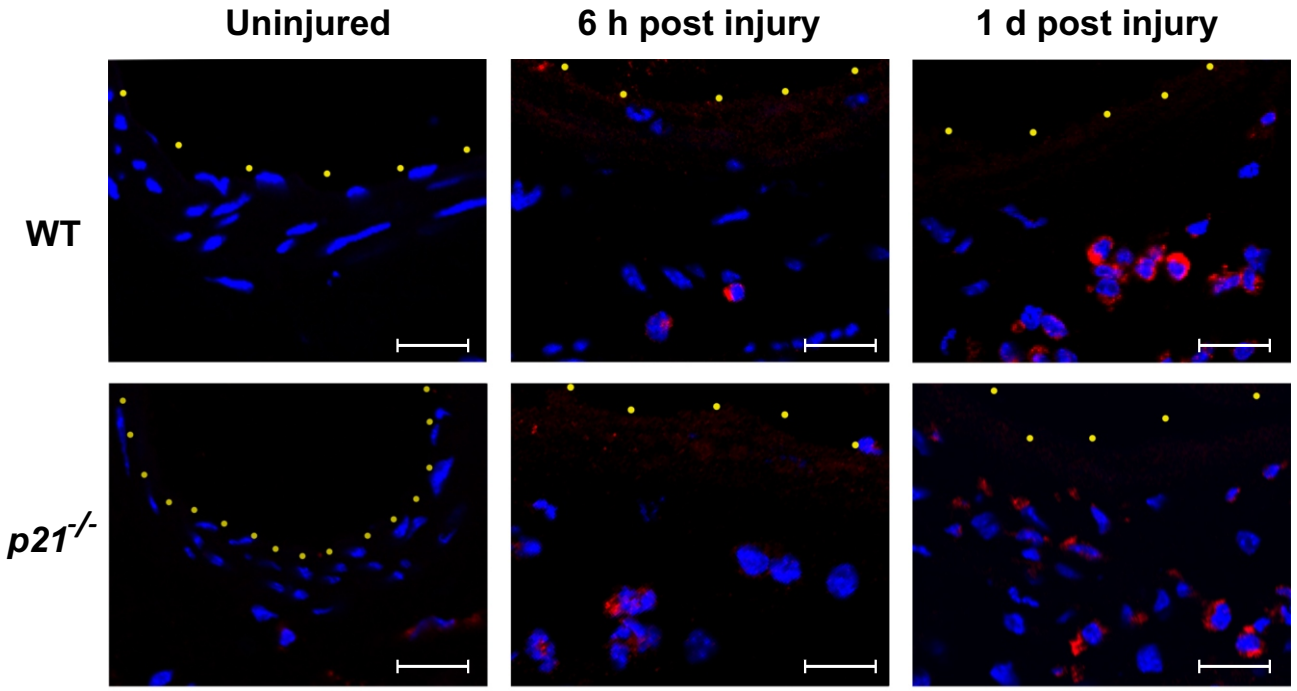

Supplemental Figure 3

Representative alternative higher-power confocal microscopic images showing CD115^{+} cells (red) in femoral artery sections from WT and *p21*$^{-/-}$ mice in uninjured vessels and at 6 h and 1 d following arterial wire injury. Nuclei (blue) were stained with DAPI. The vessel lumen (upper aspect of each panel) is marked by yellow dots. Scale bars = 20 m.

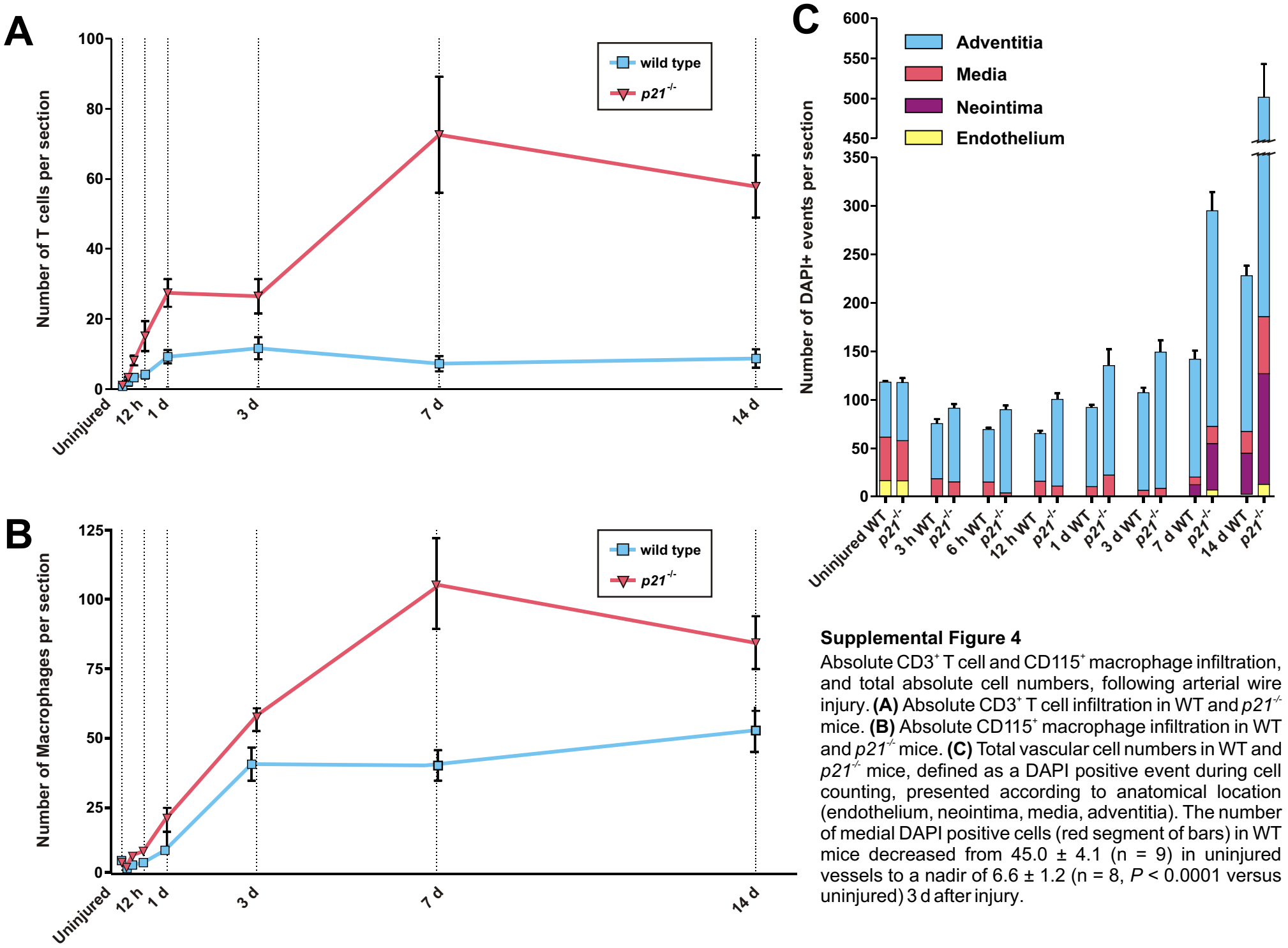

Supplemental Figure 4

Absolute $CD3^+$ T cell and $CD115^+$ macrophage infiltration, and total absolute cell numbers, following arterial wire injury. **(A)** Absolute $CD3^+$ T cell infiltration in WT and *p21*$^{-/-}$ mice. **(B)** Absolute $CD115^+$ macrophage infiltration in WT and *p21*$^{-/-}$ mice. **(C)** Total vascular cell numbers in WT and *p21*$^{-/-}$ mice, defined as a DAPI positive event during cell counting, presented according to anatomical location (endothelium, neointima, media, adventitia). The number of medial DAPI positive cells (red segment of bars) in WT mice decreased from 45.0 ± 4.1 (n = 9) in uninjured vessels to a nadir of 6.6 ± 1.2 (n = 8, $P < 0.0001$ versus uninjured) 3 d after injury.

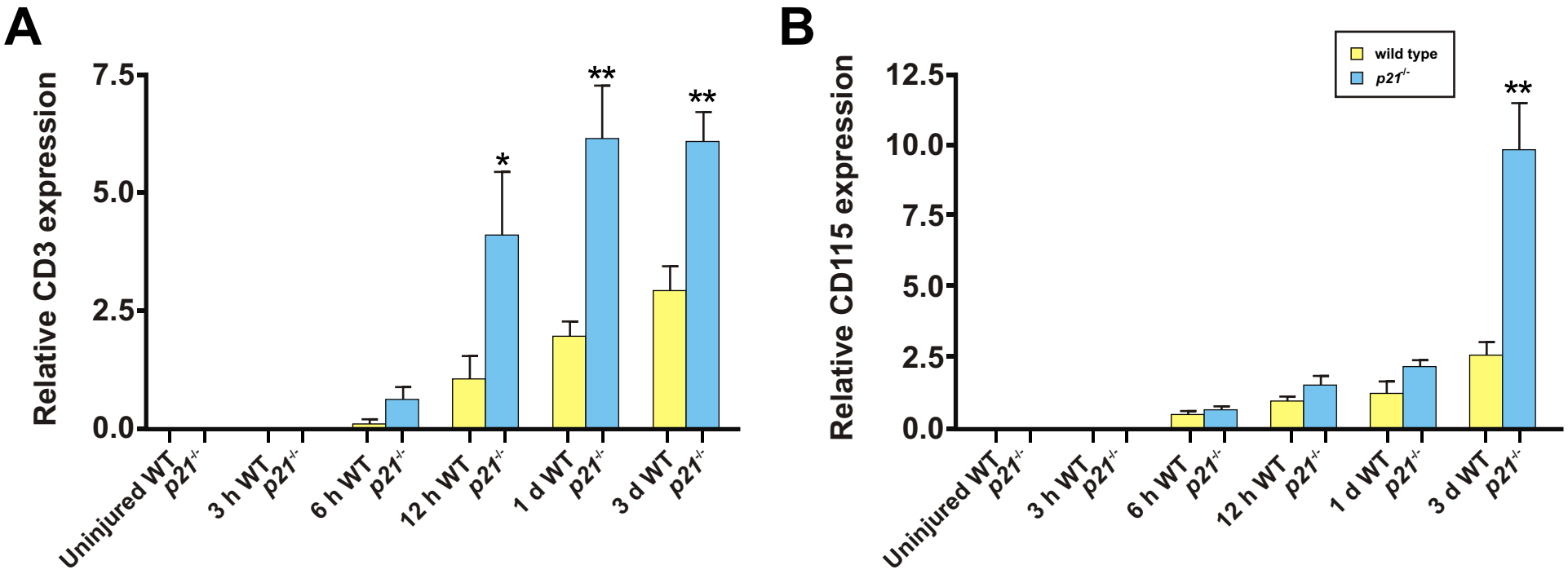

Supplemental Figure 5

Increased CD3 and CD115 local vascular mRNA levels following arterial injury. Local vascular CD3 **(A)** and CD115 **(B)** mRNA expression were assessed in uninjured vessels and after arterial injury by quantitative real time-PCR (qRT-PCR). Comparisons shown are WT versus *p21*$^{-/-}$ at each respective time-point, *$P < 0.05$, **$P < 0.005$.

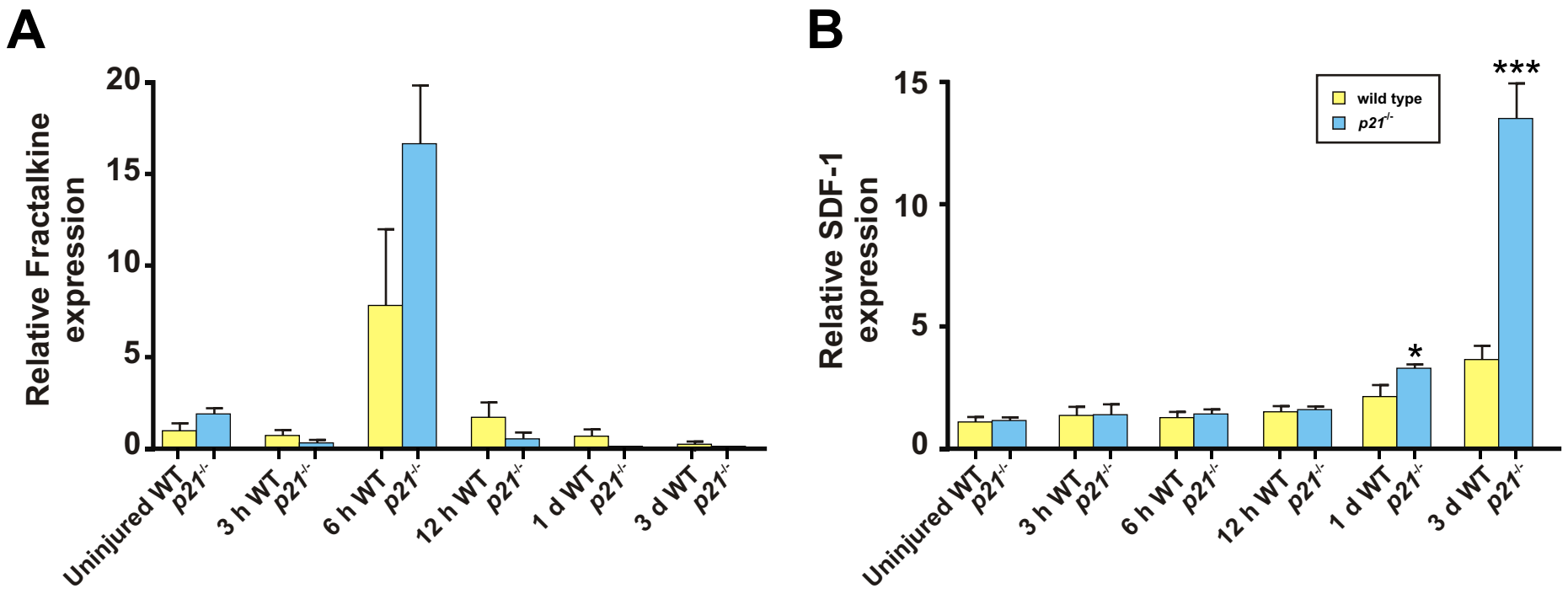

Supplemental Figure 6

Local vascular Fractalkine and SDF-1 mRNA expression following arterial injury. Local vascular Fractalkine **(A)** and SDF-1 **(B)** mRNA expression were assessed in uninjured vessels and after arterial injury by qRT-PCR. Comparisons shown are WT versus *p21*$^{-/-}$ at each respective time-point, **P* < 0.05, ****P* < 0.0005.

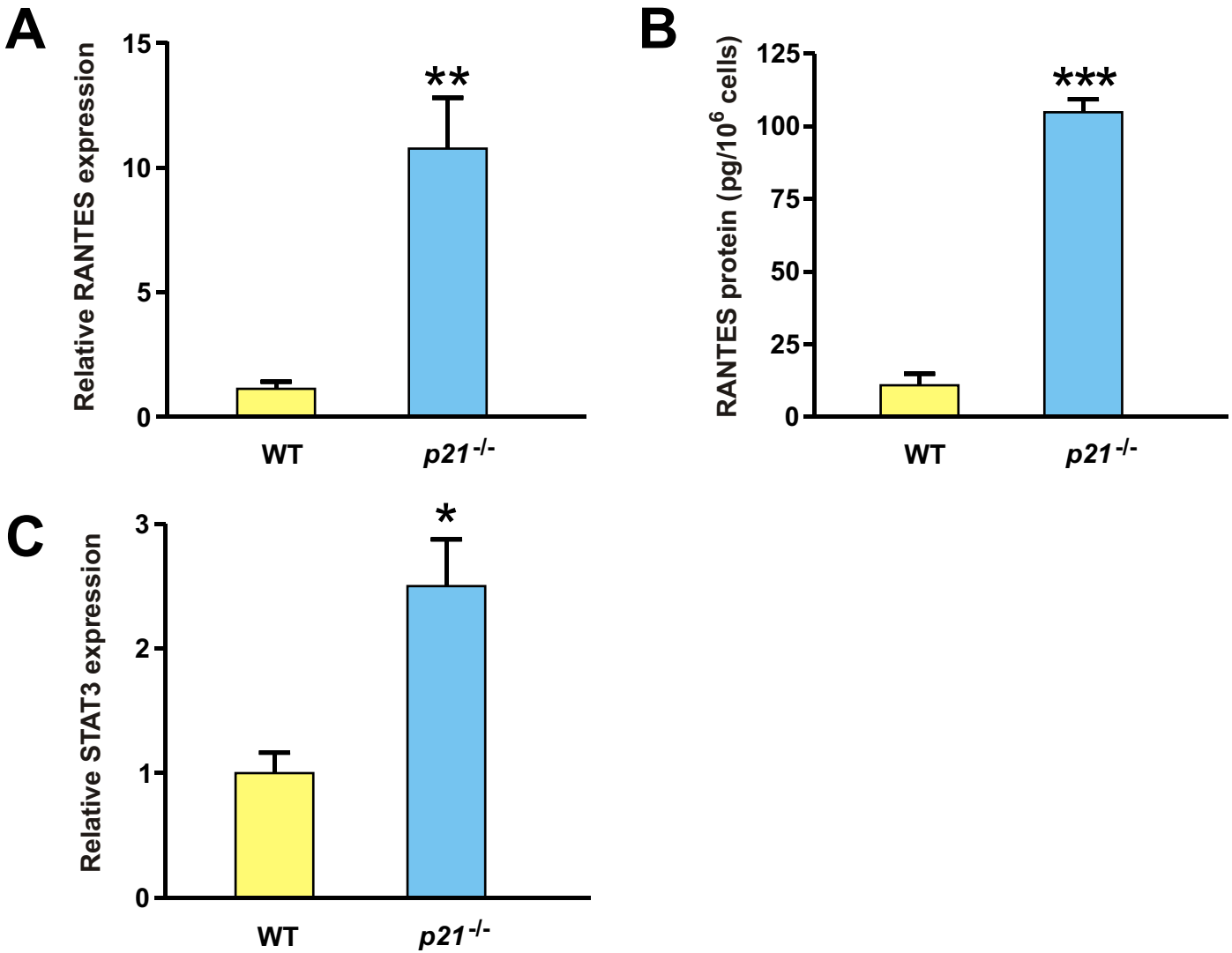

Supplemental Figure 7

p21^{Cip1} restrains both RANTES and STAT3 production in VSMCs. **(A)** Relative RANTES mRNA expression by qRT-PCR in *p21*$^{-/-}$ versus WT VSMCs (**P < 0.01, n = 3 both groups). **(B)** RANTES protein levels in supernatant from *p21*$^{-/-}$ versus WT VSMCs (***P < 0.0001, n = 3 both groups). **(C)** Relative STAT3 mRNA expression by qRT-PCR in *p21*$^{-/-}$ versus WT VSMCs (*P < 0.05, n = 3 both groups).

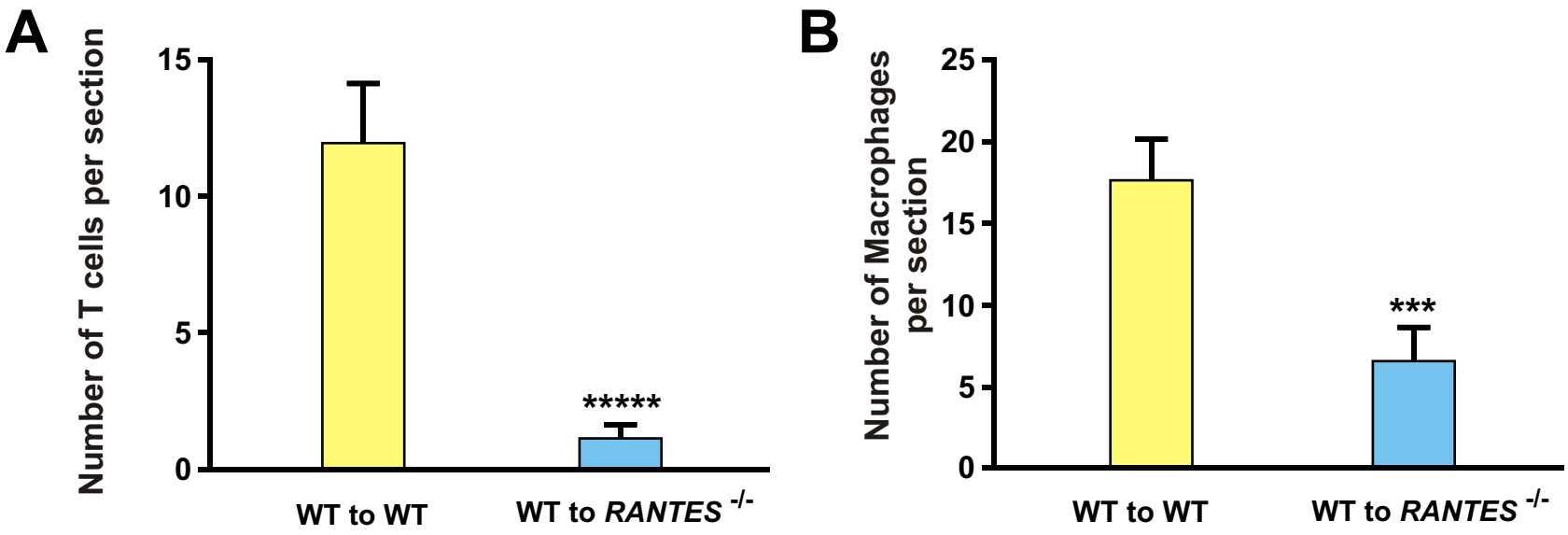

Supplemental Figure 8

Local vascular RANTES production regulates early $CD3^+$ T cell and $CD115^+$ macrophage infiltration following arterial injury. Absolute $CD3^+$ T cell **(A)** and $CD115^+$ macrophage **(B)** infiltration 1 d after arterial injury were significantly reduced in WT to *RANTES*$^{-/-}$ mice as compared to WT to WT mice (absolute $CD3^+$ T cells: *****$P < 0.0001$, n = 6 for WT to WT, n = 9 for WT to *RANTES*$^{-/-}$; absolute $CD115^+$ macrophages: ***$P < 0.005$, n = 7 for WT to WT, n = 9 for WT to *RANTES*$^{-/-}$).

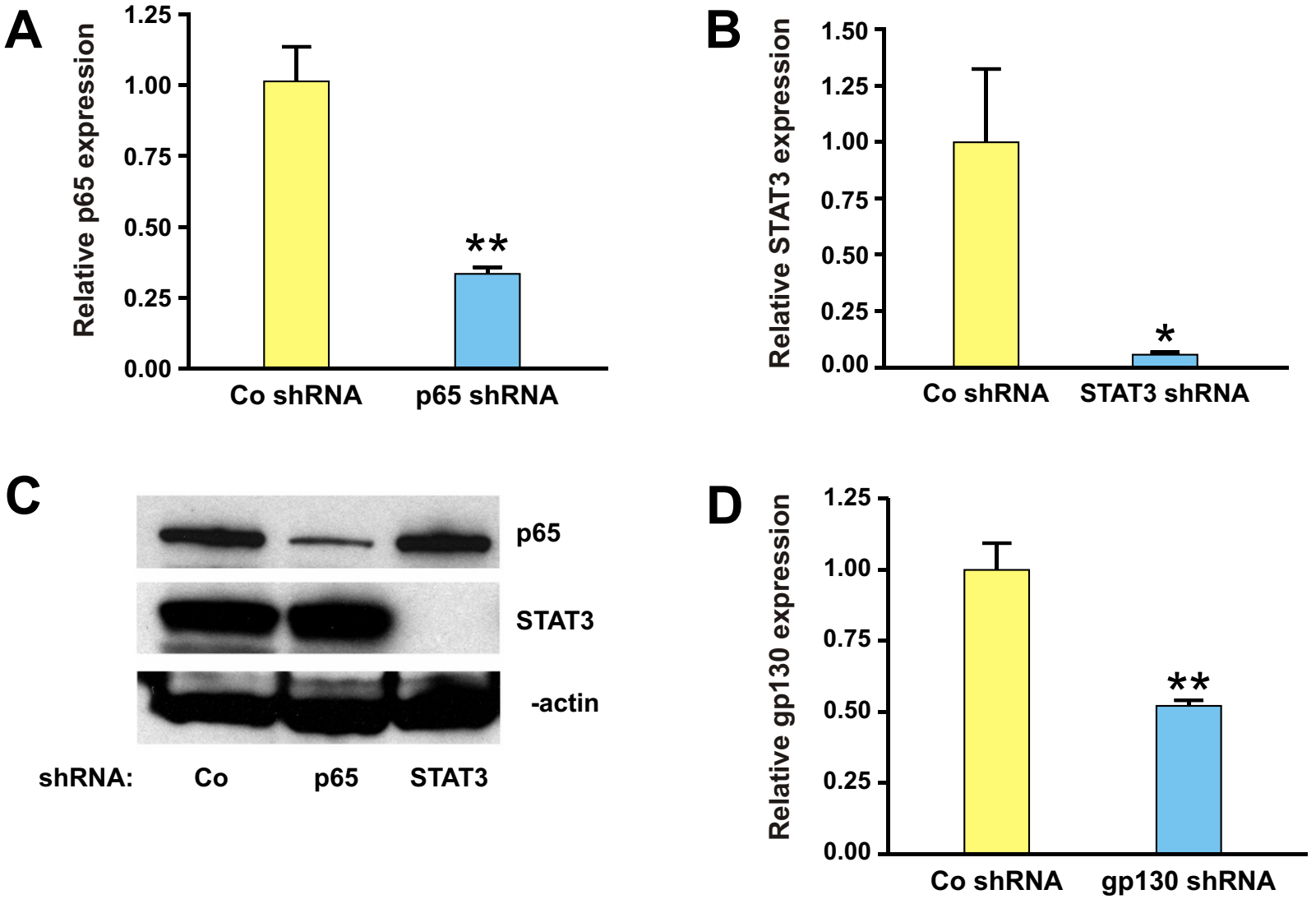

Supplemental Figure 9

Knockdown efficiency for p65, STAT3, and gp130 in WT VSMCs. **(A)** Relative p65 mRNA expression in WT Co and p65Kd VSMCs (**$P < 0.01$, n = 3 both groups). **(B)** Relative STAT3 mRNA expression in WT Co and STAT3Kd VSMCs (*$P < 0.05$, n = 4 both groups). **(C)** Corresponding WBs for p65 and STAT3 protein levels in WT Co, p65Kd and STAT3Kd VSMCs. Equal loading is shown in the lower panel by WB for -actin. **(D)** Relative gp130 mRNA expression in WT Co and gp130Kd VSMCs (**$P < 0.01$, n = 3 both groups).

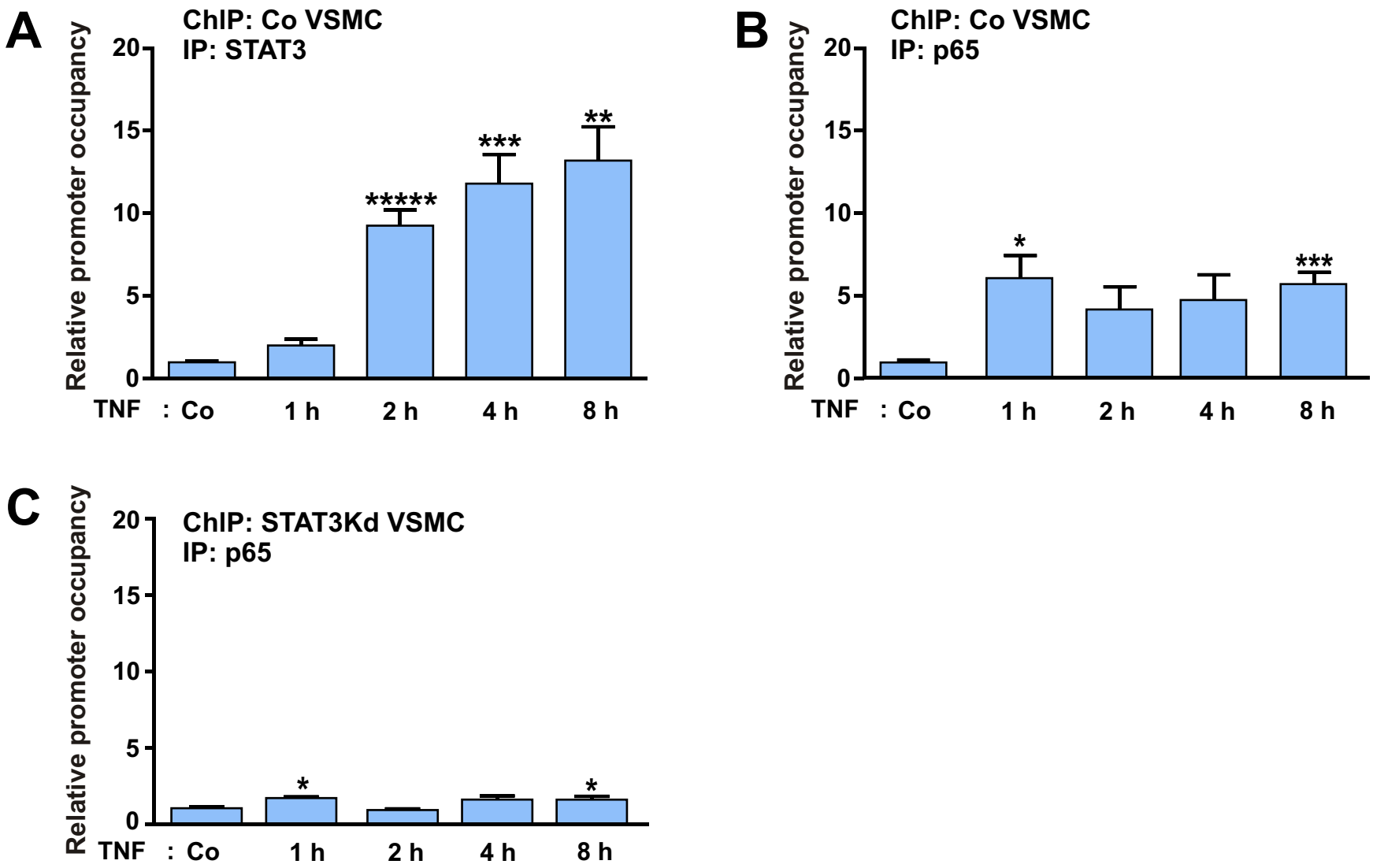

Supplemental Figure 10

Interdependent STAT3 and p65 binding to NF-kB binding site #2 of the *RANTES* promoter. **(A)** ChIP of WT Co VSMCs with IP using anti-STAT3 antibody showing STAT3 binding to NF-kB binding site #2 of the *RANTES* promoter without (Co) or with TNF stimulation for 1, 2, 4, or 8 h immediately prior to protein-DNA crosslinking (*****$P < 0.0001$, Co versus 2 h; ***$P < 0.005$, Co versus 4 h; **$P < 0.01$, Co versus 8 h; n = 3 all groups). **(B)** ChIP of WT Co VSMCs with IP using anti-p65 antibody showing p65 binding to NF-kB binding site #2 of the *RANTES* promoter following TNF stimulation (*$P < 0.05$, Co versus 1 h; ***$P < 0.005$, Co versus 8 h; n = 3 all groups). **(C)** ChIP of WT STAT3Kd VSMCs with IP using anti-p65 antibody showing p65 binding to NF-kB binding site #2 of the *RANTES* promoter following TNF stimulation (*$P < 0.05$, Co versus 1 h and Co versus 8 h; n = 3 all groups).